J Solid State Electrochem (2012) 16:2411–2418
DOI 10.1007/s10008-012-1716-5

EDITORIAL

Investigation of the microstructural features of $SrCo_{0.8}Fe_{0.2}O_{3-\delta}$ perovskite

I. V. Belenkaya · S. V. Cherepanova · A. P. Nemudry

Received: 30 December 2011 / Revised: 4 March 2012 / Accepted: 5 March 2012 / Published online: 29 March 2012

Introduction

Nonstoichiometric oxides with perovskite structure $ABO_{3-\delta}$ are the subject of intense experimental and theoretical investigations. Rapt attention to this class of materials is connected with wide possibilities of their practical application, including their use as oxygen-permeable membranes and electrodes for solid oxide fuel elements [1, 2]. It is known that grossly nonstoichiometric and doped oxides are characterized by the high concentration of structural defects (oxygen vacancies, dopant ions) and by excess Gibbs energy. Excess of energy can be reduced either due to defect ordering and their localization as structural elements (the formation of superstructures) or due to the elimination of defects from the structure with the formation of extended defects (for example, the crystallographic shear planes) [3]. An intermediate case is nanostructuring, i.e., ordering of oxygen vacancies inside nanosized domains where the defects which are excess with respect to domain structure (oxygen interstitials, vacancies) are ejected to the vicinity of the domain boundaries, where they have higher mobility [4, 5]. This phenomenon has been recognized previously as microdomain texture or microtwinning [6–9]. For materials in which high oxygen transport characteristics are required (oxygen-permeable membranes, electrodes for SOFCs), nanostructuring may play the key role because it is accompanied by the formation of the high concentration of interfaces (domain, antiphase, and twin boundaries) that can be the channels of enhanced diffusion with lower activation barriers [5, 10].

One of the materials exhibiting record-breaking oxygen permeability is perovskite having the composition $SrCo_{0.8}Fe_{0.2}O_{3-\delta}$ [11]. Investigation of the factors determining anomalously high mobility of oxygen ions in this nonstoichiometric perovskite still remains an actual problem. The aim of the present work is detailed examination of the structure and microstructure of $SrCo_{0.8}Fe_{0.2}O_{3-\delta}$ perovskite.

Experimental

Synthesis of the samples of $SrCo_{0.8}Fe_{0.2}O_{3-\delta}$ was carried out using the ceramic method described in [12]. At the final stage the samples were kept in the air at a temperature of 1,215 °C for 6 h and then slowly cooled in the furnace to the room temperature. The oxygen content of the samples was determined by means of iodometric titration. Phase transformations of $SrCo_{0.8}Fe_{0.2}O_{3-\delta}$ depending on the oxygen stoichiometry were studied at room temperature with the help of chronopotentiometry, potential step scanning and ex situ X-ray diffraction. Controllable change of the oxygen stoichiometry was achieved by means of galvanostatic oxidation/reduction in a three-electrode cell in 1 M KOH electrolyte at room temperature with polycrystalline $SrCo_{0.8}Fe_{0.2}O_{3-\delta}$ materials pressed into Pt grids along with 1% mass of Teflon as the working electrode and Ag/AgCl as the reference electrode. It was shown previously for strontium cobaltites and ferrites that the current passing through the cell is related to oxygen intercalation/deintercalation

Dedicated to Dr. Nina Zaharchuk on her 75th birthday.

I. V. Belenkaya · A. P. Nemudry (✉)
Institute of Solid State Chemistry and Mechanochemistry,
Siberian Branch of Russian Academy of Science,
630128, Novosibirsk, Russia
e-mail: nemudry@solid.nsc.ru

S. V. Cherepanova
Boreskov Institute of Catalysis Siberian Branch of Russian
Academy of Science,
630090, Novosibirsk, Russia

into/from the pristine oxide. The transferred charge n (e^-/$SrCo_{0.8}Fe_{0.2}O_{3-\delta}$) is given by the equation:

$$n = \frac{ItM}{zFm},$$

where I is current, t is time, M is molecular mass, m is the mass of sample, F is Faraday constant, z is the charge of the oxide ion. The transferred charge n is related to the amount of intercalated/deintercalated oxygen through a simple expression: $\delta=n/2$ [13, 14]. Thus, if we know the current passing through the cell and the time of the process, we can easily determine the change in oxygen nonstoichiometry.

The phase analysis of the samples was carried out by means of X-ray diffraction with Bruker D8 Advance instrument (Cu-K_α radiation). Crystal structure of the title materials was investigated by full profile Rietveld analysis of powder diffraction data in Topas V4.2 software. To study the oxidation state and coordination of iron atoms in $SrCo_{0.8}Fe_{0.2}O_{3-\delta}$, Mössbauer spectroscopy was used. The isomer shift data were given relative to the isomer shift of α-Fe. Microstructure investigation was performed by means of high resolution transmission microscopy with JEM-2010 microscope (working voltage, 200 kV; resolution, 1.4 Å). Modeling of diffraction patterns was performed with *Defect* software described in [15].

Results and discussion

According to iodometric titration, the as-prepared material had an oxygen stoichiometry corresponding to the $SrCo_{0.8}Fe_{0.2}O_{2.66}$ and specific diffraction pattern which is characterized by the presence of narrow intense reflections belonging to the structure of cubic perovskite with the parameter a_p=3.86 Å, as well as by the presence of "superstructural" weak diffuse maxima depicting the presence of periodicity in the lattice with d-spacing~$2a_p$=7.74 Å (Fig. 1). Using the full profile Rietveld analysis of powder diffraction data an attempt to refine the structure of $SrCo_{0.8}Fe_{0.2}O_{2.66}$ in unit cells for which the presence of d-spacing~$2a_p$ is characteristic was made (Table 1).

It should be stressed that refining the structure in brownmillerite cell results in "pseudo-cubic" parameters a_{BM}=c_{BM}=$\sqrt{2}a_p$=5.46 Å and b_{BM}=$4a_p$=15.47 Å. Factors R_{exp}, R_{wp}, R_p obtained as a result of full profile Rietveld analysis (Table 1), allowing to state the correctness of the chosen models, have rather low values. However, this is due to the fact that the reflections with low intensity make a smaller contribution into the values of fitting criteria. One can see in the difference curves that model X-ray diffraction patterns for the above-listed structures incorrectly describe the intensity and width of "superstructural" diffraction peaks (Fig. 2a–f).

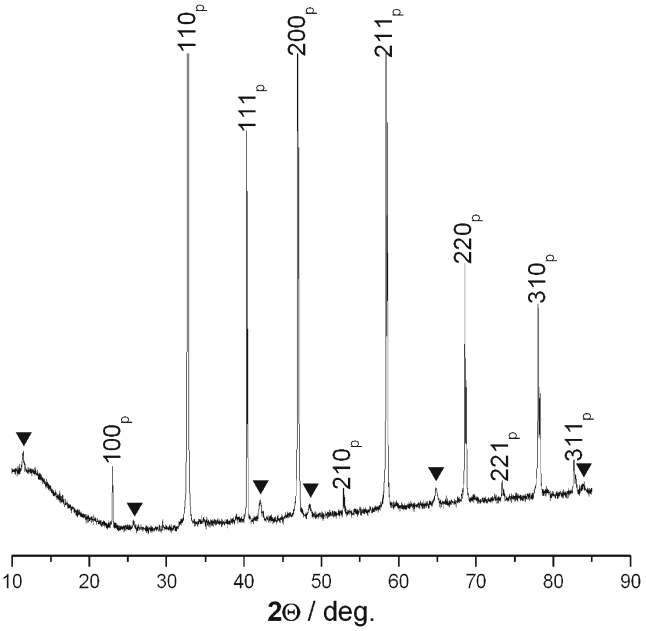

Fig. 1 X-ray diffraction patterns of the as-prepared $SrCo_{0.8}Fe_{0.2}O_{2.66}$, subscript "p" refers to the cubic perovskite cell and *filled inverted triangle* to the diffuse maxima

Since the experimental X-ray diffraction pattern is characterized by the presence of two sets of reflections having different widths and intensities, an attempt to describe the diffraction pattern with different combinations of phases with the structures shown in Table 1 was made. The best result was achieved for the two-phase system: cubic perovskite (78%) and brownmillerite (22%) with "pseudo-cubic" parameters (Fig. 2g, Table 1). In this case, diffuse maxima correspond to brownmillerite with particle size D~20 nm, while the intense reflections correspond to cubic perovskite with particle size D>100 nm.

In order to confirm this assumption, Mössbauer spectra of the sample $SrCo_{0.8}Fe_{0.2}O_{2.66}$ were recorded (Fig. 3). It is known that brownmillerites exhibit characteristic spectra: two magnetically ordered sextets (Fig. 3a) related to antiferromagnetic ordering of Fe^{3+} cations in octahedral and tetrahedral positions [13]. However, the spectrum of as-prepared material $SrCo_{0.8}Fe_{0.2}O_{2.66}$ is only composed of diamagnetic doublets; magnetically ordered sextets that would have noticeable integral intensity ~20% are absent. The obtained data are in good agreement with the data, described in [16].

Another possibility to determine whether the sample is composed of two phases offers transmission electron microscopy. However, electron diffraction patterns and high resolution images of $SrCo_{0.8}Fe_{0.2}O_{2.66}$ samples show the presence of only one brownmillerite phase. This is evidently related to the fact that under the reductive conditions of the electron microscope column, local heating of the sample by electron beam and due to anomalously high oxygen

Table 1 Structural parameters and R_{exp}, R_{wp}, R_p factors for refining the structure of $SrCo_{0.8}Fe_{0.2}O_{2.66}$ in different space groups

Space group	*a*, Å	*b*, Å	*c*, Å	R_{exp}, %	R_{wp}, %	R_p, %	GOF
$ABO_{2.5}$ (Icmm)	5.468 (5)	15.468 (6)	5.469 (4)	0.73	4.61	2.17	6.36
$ABO_{2.67}$ ($P2_1ma$)	5.466 (1)	11.606 (3)	5.469 (1)	0.73	4.41	2.24	6.08
$ABO_{2.75}$ (Cmmm)	10.942 (1)	7.728 (1)	5.471(1)	0.73	3.88	1.93	5.35
$ABO_{2.87}$ (I4/mmm)	10.941 (1)	10.941 (1)	7.729 (1)	0.73	3.91	1.73	5.39
ABO_3 (Pm3m)	3.867(1)	3.867(1)	3.867(1)	0.73	4.15	1.73	5.72
$A_2B_2O_6$ (Fm3m)	7.734(1)	7.734(1)	7.734(1)	0.73	6.70	2.64	9.23
Icmm+Pm3m	5.468 (5) 3.867(1)	15.468 (6) 3.867(1)	5.469 (4) 3.867(1)	0.73	3.95	1.65	5.45

mobility, the $SrCo_{0.8}Fe_{0.2}O_{2.66}$ material lost oxygen during examination and got transformed into brownmillerite $SrCo_{0.8}Fe_{0.2}O_{2.5}$ phase.

Convenient methods to study the phase composition of perovskite related oxides with mixed conductivity depending on oxygen stoichiometry are chronopotentiometry and potential step scanning techniques [13, 14]. To carry out electrochemical experiments, we prepared the material of the working electrode $SrCo_{0.8}Fe_{0.2}O_{2.48}$ by heating as-prepared $SrCo_{0.8}Fe_{0.2}O_{2.66}$ perovskite to 900 °C in vacuum, followed by quenching into liquid nitrogen according to the procedure described in [14]. Figure 4 shows the results of anode oxidation of $SrCo_{0.8}Fe_{0.2}O_{2.48}$ in 1 M KOH at room temperature in a three-electrode cell: change of the potential of working electrode is plotted versus the oxygen stoichiometry on Fig. 4a, and charges Δn transferred to perovskite related oxide during ΔE=10 mV potential steps are indicated in fig. 4b. By analogy with the diagrams "potential–charge transfer" obtained previously for $SrCoO_{2.5+x}$ and $SrFeO_{2.5+x}$ [13, 14], four characteristic regions can be distinguished in the curves "E−3−δ" for $SrCo_{0.8}Fe_{0.2}O_{2.48+x}$ (Fig. 4a). Region I ($2.48<3-\delta<2.52$), in which a monotonous increase in potential from –50 to 100 mV occurs, is related to the formation of solid solutions. Region II ($2.52<3-\delta<2.75$), in which the potential of the working electrode

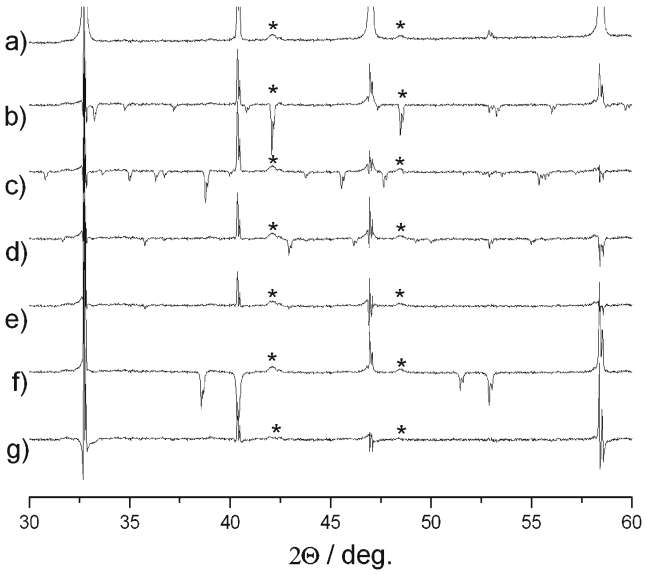

Fig. 2 Experimental powder X-ray diffraction pattern of as-prepared $SrCo_{0.8}Fe_{0.2}O_{2.66}$ (*a*) and the difference curves between the experimental and theoretical X-ray diffraction patterns calculated for: (*b*) orthorhombic brownmillerite $ABO_{2.5}$ (Icmm), (*c*) Grenier phase $ABO_{2.67}$ ($P2_1ma$), (*d*) orthorhombic perovskite $ABO_{2.75}$ (Cmmm), (*e*) tetragonal perovskite $ABO_{2.87}$ (I4/mmm), (*f*) double perovskite (Fm3m), (*g*) two-phase pattern: perovskite (Pm3m) + brownmillerite (Icmm). The *asterisks* refer to the diffuse maxima

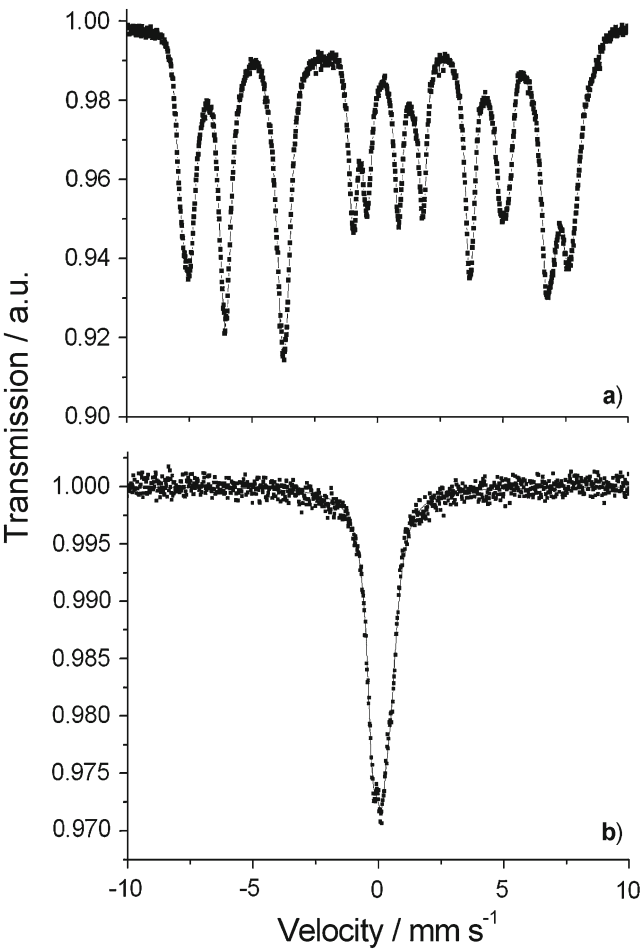

Fig. 3 Mössbauer spectra of vacuum-quenched $SrCo_{0.8}Fe_{0.2}O_{2.48}$ brownmillerite (**a**) and as-prepared $SrCo_{0.8}Fe_{0.2}O_{2.66}$ (**b**)

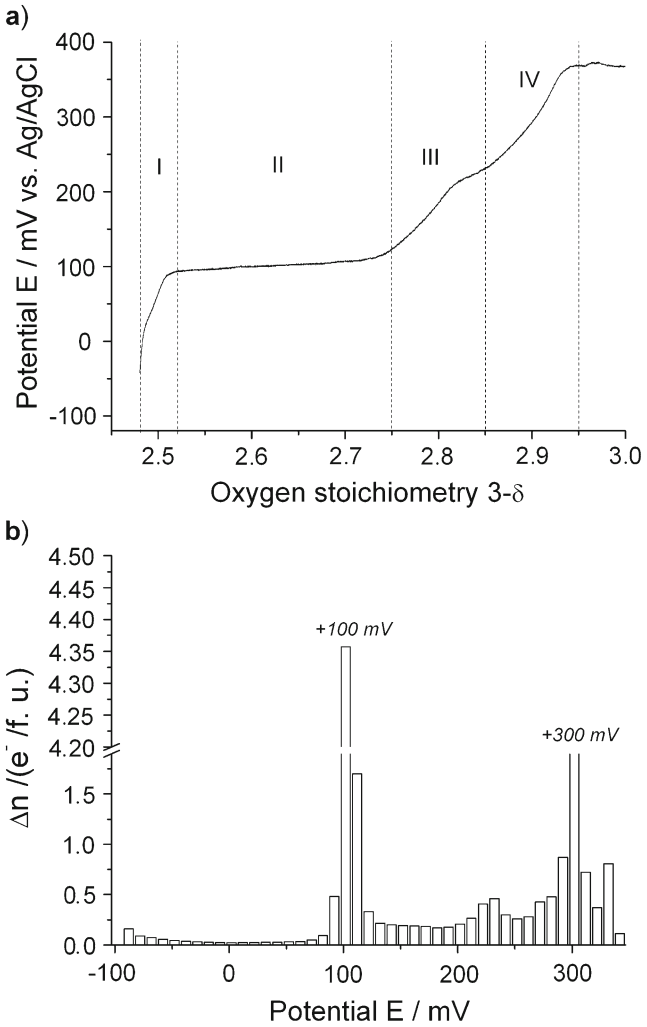

Fig. 4 **a** Galvanostatic anodic oxidation of quenched in vacuum perovskite $SrCo_{0.8}Fe_{0.2}O_{2.48}$ at 300 K in 1 M aqueous KOH electrolyte: change of potential E with charge transfer n; **b** Anodic oxidation of $SrCo_{0.8}Fe_{0.2}O_{2.48}$: potential step scanning mode. Δn charge transferred per potential step

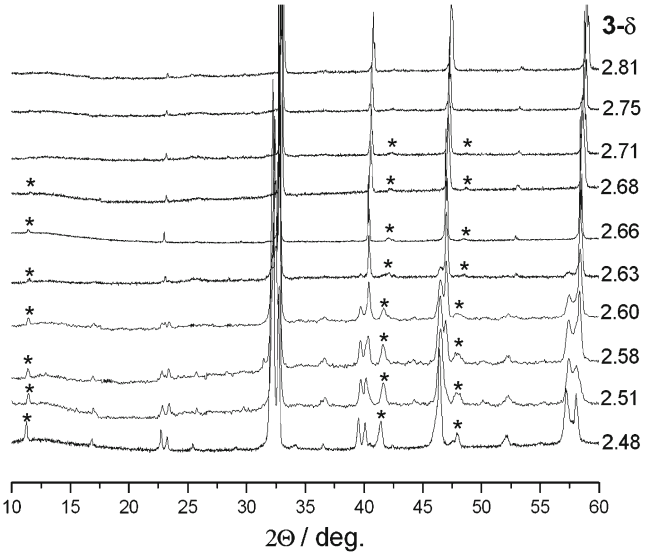

Fig. 5 Ex situ X-ray diffraction data for the samples with different oxygen content $3-\delta$, obtained by electrochemical oxidation of vacuum-quenched $SrCo_{0.8}Fe_{0.2}O_{2.48}$ sample. The *asterisks* refer to the diffuse maxima

remains almost constant (E~100 mV) with an increase in the oxygen content of the sample, depicts the oxidation in two-phase mode. Regions III ($2.75<3-\delta<2.87$) and IV ($2.87<3-\delta<3.0$) appear to be characterized by a continuous increase of the potential from E~100 mV to E~370 mV with different slopes; this corresponds to further oxidation with the formation of different intermediate phases. For us, the most interesting fact is that the oxygen stoichiometry $3-\delta=2.66$ corresponds to the two-phase region of oxidation, which agrees with the data of XRD phase analysis (Table 1).

To obtain detailed information about the phase composition of the products of anode oxidation of $SrCo_{0.8}Fe_{0.2}O_{2.48}$ in the galvanostatic mode, we carried out ex situ X-ray diffraction measurements (Fig. 5). Starting material with oxygen stoichiometry $3-\delta=2.48$ has brownmillerite structure with parameters: $a=5.58$ Å, $b=15.75$ Å, $c=5.47$ Å. The calculation of the coherence length from the half widths of reflections gives D~75 nm, which agrees with the electron microscopic data (Fig. 6). Evaluation of ex situ X-ray data shows that an increase in oxygen stoichiometry in the region I from 2.48 to 2.52 is accompanied by a noticeable decrease in the unit cell parameters (Fig.7b), which is in agreement with the electrochemical data and provides evidence of the existence of the homogeneity region of brownmillerite phase $SrCo_{0.8}Fe_{0.2}O_{2.5\pm x}$ (x~0.02).

Further increase in the oxygen content of the sample (region II, $2.52<3-\delta<2.75$) with accordance to the two-phase mode of oxidation results in to a monotonous decrease in intensity and increase in width of brownmillerite reflections whereas intensity of narrow perovskite reflections grows. The XRD patterns of electrochemically oxidized samples with oxygen stoichiometry $3-\delta=2.66$ and 2.68 are similar to the diffraction pattern of as-prepared $SrCo_{0.8}Fe_{0.2}O_{2.66}$ material and contain in addition to intensive peaks related to perovskite diffuse maxima in the region of reflections (020), (121), (161), (222), (1 10 1) of brownmillerite.

It should be noted that constant unit cell parameters of orthorhombic brownmillerite and cubic perovskite phases in region II demonstrate considerable difference (Fig. 7b). However, with approach to the composition $3-\delta=2.66$ we observe a decrease in orthorhombic distortions; as a result, for the samples with oxygen stoichiometry $3-\delta=2.66$–2.68 the brownmillerite phase has pseudo-cubic cell with the parameters coinciding with the parameters of the perovskite phase (Fig. 7b). Estimation of the coherence length (D) of brownmillerite phase within the region II by means of

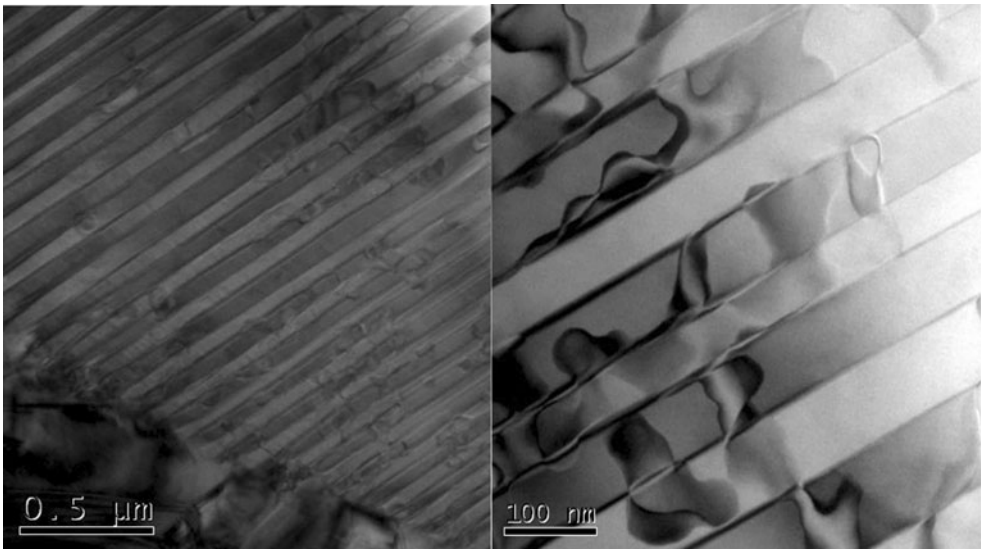

Fig. 6 Dark field images of vacuum-quenched $SrCo_{0.8}Fe_{0.2}O_{2.48}$ sample demonstrating the formation of twins and antiphase domains of 70–100 nm in size

Williamson–Hall method using reflections *0k0* shows that *D* in the direction [010] decreases from 75 to 15 nm (Fig. 7c). With further increase in the oxygen content of the sample, the intensity of brownmillerite reflections decreases so substantially that is no longer suitable for processing, and then runs down into the background.

The diffraction patterns from regions III and IV ($2.75<3-\delta<2.87$; $2.87<3-\delta<3$) can be indexed in the cubic perovskite cell but these regions are out of the interest for the present work and will be studied in more detail later, and the results will be published separately.

Thus, the set of obtained data can be interpreted in the following manner. With a decrease in the oxygen content of $SrCo_{0.8}Fe_{0.2}O_{3-\delta}$ the oxygen stoichiometry is realized through the formation of MO_5 pentahedrons and MO_4 tetrahedrons located randomly; the cubic perovskite structure with space group Pm3m is conserved. With the achievement of the critical oxygen stoichiometry $3-\delta<2.75$ vacancies get

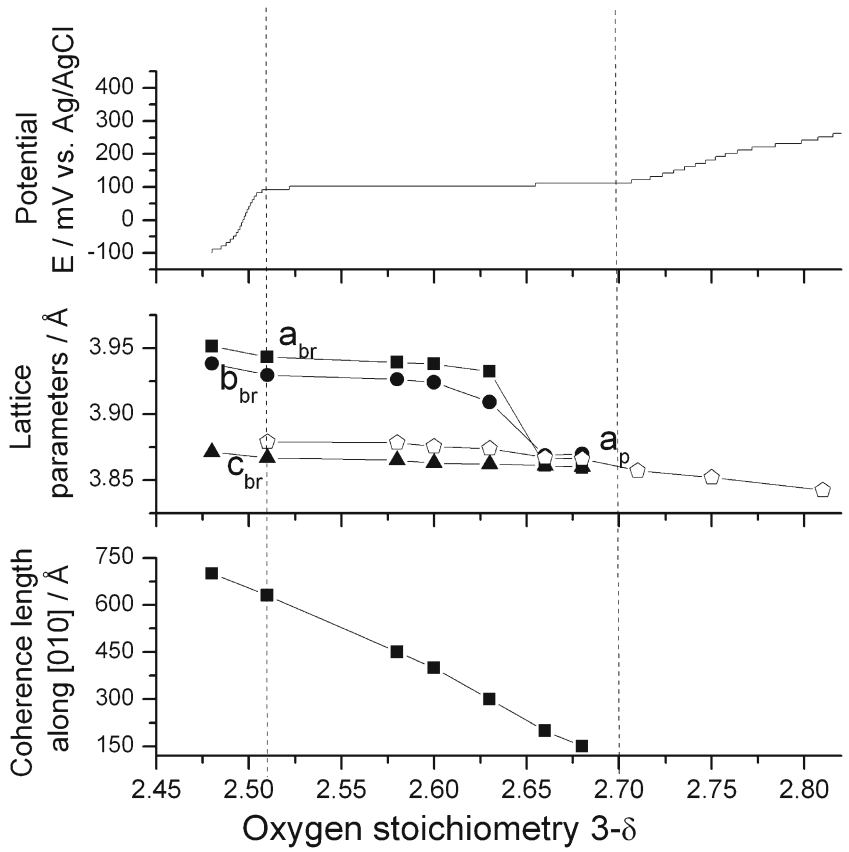

Fig. 7 Data on the electrochemical oxidation of vacuum-quenched $SrCo_{0.8}Fe_{0.2}O_{2.48}$ sample: **a** curve "E-3 $-\delta$", obtained by potential step scanning techniques; **b** perovskite and reduced brownmillerite unit cell parameters evaluated from ex situ X-ray diffraction data; **c** coherence length in [010] direction of brownmillerite phase

ordered. The formation of superstructures may proceed via nanostructuring: the precipitation of nanosized brownmillerite domains that are coherently jointed with the perovskite matrix, that is evidenced by the close structural parameters of "pseudo-cubic" brownmillerite and perovskite (Fig. 7b). Further decrease in oxygen content, as ex situ X-ray diffraction studies showed, leads to an increase in the size of brownmillerite domains and to subsequent transformation of perovskite $SrCo_{0.8}Fe_{0.2}O_{3-\delta}$ ($3-\delta=2.75$) into brownmillerite $SrCo_{0.8}Fe_{0.2}O_{2.5\pm x}$ ($x\sim0.02$) in the course of two-phase transformation.

The absence of magnetically ordered components (characteristic of brownmillerite structure) in the Mössbauer spectrum of $SrCo_{0.8}Fe_{0.2}O_{2.66}$ allows us to assume that the title material is not simply a two-phase system but a microheterogeneous compound with coherently jointed domains of different composition (…OTOTO…OO…OTO…), in which the magnetic long-range order is distorted by the alternation of brownmillerite (OTOT…) and perovskite (OOO…) layers. The presence of diamagnetic slabs of oxygen-deficient perovskite separating antiferromagnetic brownmillerite layers destroys magnetic ordering in the nanostructured sample. It should be noted that the Mössbauer spectrum of $SrCo_{0.8}Fe_{0.2}O_{2.66}$ differs from the Mössbauer spectrum of the sample with composition $SrFeO_{2.66}$, previously published in [13], for which the magnetically ordered sextets of brownmillerite were observed. Obviously, the difference in these spectra is due to the presence of 63% Co^{3+} ions in $SrCo_{0.8}Fe_{0.2}O_{2.66}$, according to [16], which is characterized by low-spin state, that may cause further weakening of the magnetic ordering in the microheterogeneous system.

To confirm the proposed microstructure of the as-prepared sample, we carried out modeling of X-ray diffraction patterns using Debye equation. In the model, perovskite layers $ABO_{3-\delta}$ (…OOO$-\delta$…) were coherently stacked with brownmillerite layers (…OTOT′…) along the direction [010]. To fulfill the coherence condition, lattice parameters of brownmillerite and perovskite phases are to meet the requirement: $a_{BM}=c_{BM}=\sqrt{2}a_p$ and $b_{BM}=4a_p$, which agrees with the diffraction data (Fig. 7b). To join the phases in the plane [101], we used a cell constructed on the diagonals of perovskite cell.

It is known that different ordering of tetrahedral chains is characteristic of the brownmillerite structure, which in turn leads to different space symmetry groups: Icmm, Ibm2, and Pnma [17]. Figure 8 shows the results of modeling the diffraction patterns using different space groups. One can see that the best correspondence is achieved for space group Icmm with statistic ordering of right and left tetrahedral chains along b axis. Taking into consideration the oxygen stoichiometry of as-prepared material $3-\delta=2.66$ and the fact that the neighboring phases (according to the electrochemical oxidation data, Fig. 4) are $SrCo_{0.8}Fe_{0.2}O_{2.75}$ and $SrCo_{0.8}Fe_{0.2}O_{2.5}$, the phase relationship of the sample is $W(O-\delta)\div W(OTOT')=64\div36$. Further, taking into account the fact that the size of brownmillerite cell along b axis (OTOT′) is about four times as large as that of the perovskite cell (O), we calculated the probability of the appearance of OTOT' and O layers using the equation:

$$\frac{W(O-\delta)}{W(OTOT')}=\frac{64}{36}=\frac{x\cdot y}{4x\cdot(1-y)},$$

where y is the probability of the perovskite layer (O$-\delta$), $(1-y)$ is the probability of brownmillerite layer (OTOT′), x is the size of the perovskite cell along b axis. The calculated probabilities were 0.87 for the layers with the perovskite structure (O$-\delta$) and 0.13 for the layers with the brownmillerite structure (OTOT′). Variation of layer thickness showed that the best correspondence is observed for the thickness of 20 nm for brownmillerite phase and 80 nm for perovskite phase, which agrees with the experimentally determined coherence lengths.

Similar nanostructuring phenomena were observed previously for nonstoichiometric ferrites with perovskite structure characterized by oxygen content $2.5<3-\delta<2.7$ [6–9]. Because the mobility of oxygen in ferrites is lower by an order of magnitude than that in $SrCo_{0.8}Fe_{0.2}O_{3-\delta}$, for systems $SrFe_{1-x}V_xO_{2.5+x}$ ($x=0.05$, 0.1) [6] and $SrFe_{1-x}Mo_xO_{2.5+3/2x}$ ($x=0.05$) [8], as well as $SrCo_{1-x}Al_xO_{2.5+x}$ [7] and $CaTi_{0.4}Fe_{0.6}O_{3-\delta}$ [9] the occurrence of nanostructuring in perovskites through the formation of coherent 90° brownmillerite domains randomly disoriented in six directions was

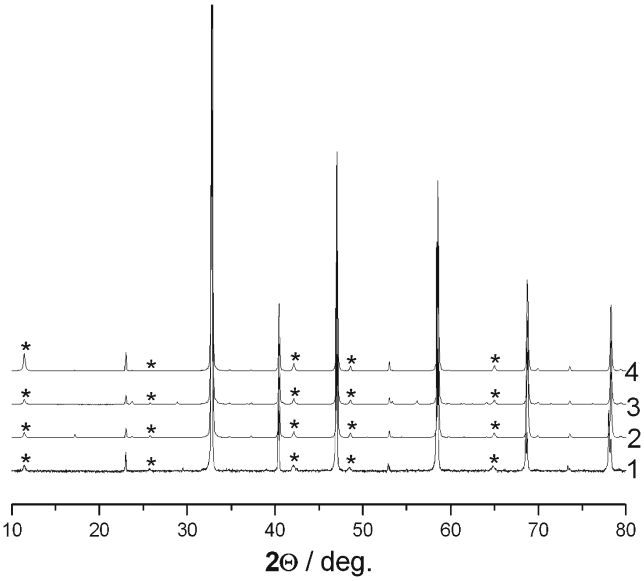

Fig. 8 Comparison of experimental XRD pattern of $SrCo_{0.8}Fe_{0.2}O_{2.66}$ (*1*) with modeling data obtained by the alternation of oxygen-deficient cubic perovskite (S. G. Pm3m) and brownmillerite with space groups Ibm2 (*2*), Pcmn (*3*), and Icmm (*4*). The *asterisks* refer to the diffuse maxima

confirmed visually using transmission electron microscopy. The proposed model of nanostructuring related to 1D disorder along the direction [010] does not contradict microtwinning described for ferrites, because the domain boundary jointing differently orientated domains can be formed only by distortions in the OTOT′ sequence of octahedral and tetrahedral layers. Attempt to describe the microstructure of the title material by means of the 3D model (90° randomly disoriented brownmillerite domains) is planned for further investigation.

As we have noted in the "Introduction" section, for oxygen-deficient perovskites in the case of high concentration of oxygen vacancies, their ordering with the formation of stoichiometric superstructures $ABO_{3-1/n}$, where n=2, 4, 8÷∞ takes place [18]. For perovskites with oxygen content corresponding to the two-phase region $1/n<\delta<1/(n+1)$ (either in result of redox process or aliovalent doping), as we demonstrated in this work and previously [6, 8], nanostructuring, i.e., the formation of nanosized coherently jointed domains having the composition $ABO_{3-1/n}$ and $ABO_{3-1/n+1}$ is characteristic feature. It may be assumed that this process sequentially takes place as the oxygen content of the sample changes, within the whole range of oxygen stoichiometry. This may be of principal importance for oxygen mobility in nonstoichiometric perovskites because domain boundaries differ from the bulk material in their transport properties [10] and are either high diffusivity pathways or barriers for ion migration.

Generally, it is believed that the oxygen sublattice in perovskites at elevated temperatures becomes disordered and nanostructuring effects observed at low temperatures are not related to the high-temperature oxygen transport. In this respect it should be noted that J.-C. Grenier and P. Hagenmuller in [19] have proposed a high-temperature structure of the "cubic" $SrFeO_{2.5+x}$ perovskite, consisting of disoriented brownmillerite-type domains with oxygen excess localized in the domain walls. This assumption was confirmed by M. Takano by means of high-temperature Mossbauer spectroscopy [20]. In [21], S. Adler, with the help of high-temperature NMR, showed the co-existence of both mobile and immobile oxygen ions in the perovskites at T>800 °C, this fact is also in agreement with the model of microdomain structure of high-temperature perovskite phases. The high-temperature X-ray diffraction data for $SrFeO_{3-z}$ and $SrFe_{1-x}Mo_xO_{3-z}$, described in [22, 23] provide evidence that the stability of vacancy-ordered phases increases with increasing vacancy concentration, as a result, the structure of brownmillerite and nanodomains texture based on it are stable at low oxygen partial pressures up to T ~1,200 °C. It was also shown in [24] that the brownmillerite structure $SrCo_{0.8}Fe_{0.2}O_{2.5}$ is stable in vacuum (P~10^{-5} atm) at high temperatures (T~1,200 °C). Thus, effects of nanostructuring based on the stability of brownmillerite-type domains at low oxygen partial pressure have to be considered in the study of high-temperature oxygen transport in oxygen-permeable membranes and SOFC electrodes.

Conclusion

Specific powder X-ray diffraction pattern of the as-prepared $SrCo_{0.8}Fe_{0.2}O_{2.66}$ membrane materials, characterized by the presence of narrow intense perovskite reflections, and weak diffuse brownmillerite maxima can be described correctly as a two-phase system: cubic perovskite (78%) and "pseudo-cubic" brownmillerite (22%) with particle size D>100 nm and D~20 nm, respectively. On the basis of examination of the phase composition depending on oxygen stoichiometry with the help of chronopotentiometry, potential step scanning techniques, ex situ X-ray diffraction measurements and Mössbauer spectroscopy data, we propose a model of nanostructuring of $SrCo_{0.8}Fe_{0.2}O_{2.66}$ material. In the model, the slabs of perovskite $ABO_{3-\delta}$ (..OOO−δ..) are coherently jointed with brownmillerite layers $A_2B_2O_5$ (..OTOT…) along the direction [010]. In order to meet the condition of coherence, cell parameters for brownmillerite and perovskite obey the relations: $a_{BM}=c_{BM}=\sqrt{2}a_p$ and $b_{BM}=4a_p$, which agrees with the experimental diffraction data. The proposed model of nanostructured $SrCo_{0.8}Fe_{0.2}O_{2.66}$ is in agreement with the results of full profile modeling of diffraction patterns by means of the Debye equation.

References

1. Bouwmeester HJM, Burggraaf AJ (1996) Dense ceramic membranes for oxygen separation. In: Burggraaf AJ, Cot L (eds) Fundamentals of inorganic membrane science and technology. Elsevier, Amsterdam, pp 435–528
2. Sunarso J, Baumann S, Serra JM, Meulenberg WA, Liu S, Lin YS, da Costa JC Diniz (2008) J Membrane Sci 320:13–41
3. Anderson JS, Rabenau A (1970) Problems of Nonstoichiometry. Part 1. North-Holland, Amsterdam
4. Nemudry A, Zyryanov V (2011) Nanostructured perovskites for the fabrication of thin ceramic membranes and related phenomena. In: Basile A, Gallucci F (eds) Membranes for membrane reactors: preparation, optimization, and selection. Wiley, United Kigdom, pp 201–227
5. Nemudry A, Uvarov N (2006) Solid State Ionics 177:2491–2494
6. Nakayama N, Takano M, Inamura S, Nakanishi N, Kosuge K (1987) J Solid State Chem 71:403–417
7. Lindberg F, Svensson G, Istomin S, Aleshinskaya S, Antipov E (2004) J Solid State Chem 177:1592–1597
8. Markov A, Savinskaya O, Patrakeev M, Nemudry A, Leonidov I, Pavlyukhin Yu, Ishchenko A, Kozhevnikov V (2009) J Solid State Chem 182:799–806
9. Canales-Vazquez J, Figueiredo F, Waerenborgh J, Zhou W, Frade J, Irvine J (2004) J Solid State Chem 177:3105–3113
10. Lee W, Salje E, Bismayer U (2003) J Phys Condens Matter 15:1353–1366

11. Bouwmeester HJM, Burggraaf AJ (1997) Dense ceramic membranes for oxygen separation. In: Gellings PJ, Bouwmeester HJM (eds) CRC handbook of solid state electrochemistry. CRC, Enschede, pp 481–553
12. Pyatiletova E, Nemudry A, Lyakhov N (2007) Inorg Mater 43:1–8
13. Nemudry A, Weiss M, Gainutdinov I, Boldyrev V, Schöllhorn R (1998) Chem Mater 10:2403–2411
14. Nemudry A, Rudolf P, Schöllhorn R (1996) Chem Mater 8:2232–2238
15. Cherepanova S, Tsybulya S (2000) J Mol Catal A Chem 158:263–266
16. Pokholok K, Presnyakov I, Ketso V, Oleinikov N, Kuznetsov N (2001) Russ J Coord Chem 27:632–635
17. D'Hondt H, Abakumov A, Hadermann J, Kalyuzhnaya A, Rozova M, Antipov E, Tendeloo V (2008) Chem Mater 20:7188–7194
18. Karvonen L, Yoon S, Hug P, Yamauchi H, Weidenkaff A, Karppinen M (2011) Mater Res Bull 46:1340–1345
19. Grenier J, Ea N, Pouchard M, Hagenmuller P (1985) J Solid State Chem 58:243–252
20. Takano M, Okita T, Nakayama N, Bando Y, Takeda Y, Yamamoto O, Goodenough J (1988) J Solid State Chem 73:140–150
21. Adler S, Russek S, Reimer J, Fendorf M, Stacy A, Huang Q, Santoro A, Lynn J, Baltisberger J, Werner U (1994) Solid State Ionics 68:193–211
22. Savinskaya O, Nemudry A, Nadeev A, Tsybulya S, Lyakhov N (2010) Bulletin of the Russian Academy of Sciences. Physics 74:1053–1054
23. Savinskaya O, Nemudry A (2011) J Solid State Electrochem 15:269–275
24. Podyacheva O, Ismagilov Z, Shmakov A, Ivanov M, Nadeev A, Tsybulya S, Rogov V (2009) Catal Today 147:270–274